SURFACE WAVES IN ARCTIC SEAS, OBSERVED FROM TERRASAR-X

Johannes Gemmrich[*] [a] *Andrey Pleskachevsky, Susanne Lehner*[*] [b] *Erick Rogers*[*] [c]

[a] University of Victoria
Physics & Astronomy
Victoria, BC, Canada
[b] German Aerospace Center (DLR), FMS
Bremen, Germany
[c] Naval Research Laboratory
Stennis Space Center, Mississippi, USA

ABSTRACT

The need for wide-spread, up-to-date sea state observations in the emerging ice-free Arctic will further increase as the region will open up to marine operations. Here we present an example of spatial wave field parameters obtained from a TerraSAR-X StripMap swath in the southern Beaufort Sea. Significant wave heights varied from $< 1m$ to $> 2.2m$ over distances of less than 50km. These results are compared to current state-of-the-art implementation of spectral wave prediction models. Overall, good agreement is observed, and limitations of the remote sensing algorithm and the wave model are highlighted.

Index Terms— Wave retrieval from SAR. Arctic sea state. Wavewatch III model - remote sensing comparison.

1. INTRODUCTION

The reduction of the sea ice coverage during the boreal summer will lead to an increased importance of wind waves for the dynamic processes of the Arctic Seas. The large ice free areas lead to longer fetch and thus longer and higher sea state [1]. Wind waves will enhance upper ocean mixing, may affect the breakup of ice sheets, and will likely lead to increased coastal erosion. Our long-term goal is a better understanding of the two-way interaction of waves and sea-ice, in order to improve wave models as well as ice models applicable to a changing Arctic wave- and ice climate.

Observations of surface wave properties are commonly obtained with long-term moorings equipped with surface wave buoys [2] or sub-surface upward-looking acoustic Doppler profilers [1]. However, the need for annual recovery and redeployments makes surface moorings impractical in seasonally ice-covered waters. Wave information from sub-surface instrumentation is commonly only available after the instrument recovery. Therefore, the sea state in the open waters of the Arctic Ocean is currently not monitored on a regular basis. Remote sensing methods can provide a viable alternative to in-situ wave observations, in particular in arctic seas. Here, we utilize information retrieval from space-borne SAR imagery. This information will complement and validate model data for the spatial and temporal evolution of sea state in the Arctic.

2. METHODS

Over the ocean, synthetic aperture radar is capable of providing wind and wave information by measuring the roughness of the sea surface, as well as providing information on ice coverage. In particular, TerraSAR-X data have been used to investigate the highly variable wave climate in coastal areas [3],[4],[5]. However, the use of these data at the sea ice boundary is still to be utilized in full detail. In addition, TerraSAR-X data provide accurate estimates of the wind field over the ocean as well as the position of the ice edge, ice drift estimates, and floe size distributions.

We are using data from the X-band high resolution SAR satellite TerraSAR-X (TS-X), and its twin, TanDEM-X (TD-X). They operate with 31mm wavelength from 15 sun-synchronous orbits per day at 514km. The repeat-cycle is 11 days, but in polar regions the same region can usually be imaged daily, with different incidence angles. The coverage and resolution depends on the choice of various satellite modes: Wide ScanSAR mode covers 450km by 250km with about 40m resolution. ScanSAR mode covers a 100km wide swath, StripMap mode covers 30km width with a resolution of about 2.5m, and the Spotlight node covers 10km by 10km with a resolution of about 1m. The (Wide)ScanSAR modes are best suited for monitoring the large scale ice field characteristics. Wave and wind parameters are best observed with StripMap mode and VV-polarization.

[*]Funding for this work was provided by the US Office of Naval research under the DRI "Sea-state and boundary layer processes in the emerging Arctic".

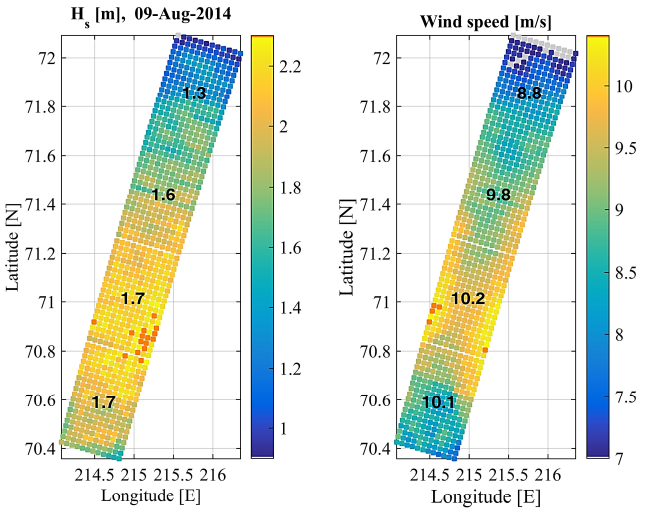

Fig. 1. Spatial heterogeneity of significant wave height H_s (left) and wind speed u (right). Colour fields show results retrieved from TerraSAR-X Stripmap images, black numbers give wind speed input values and calculated wave heights for Wavewatch III model results.

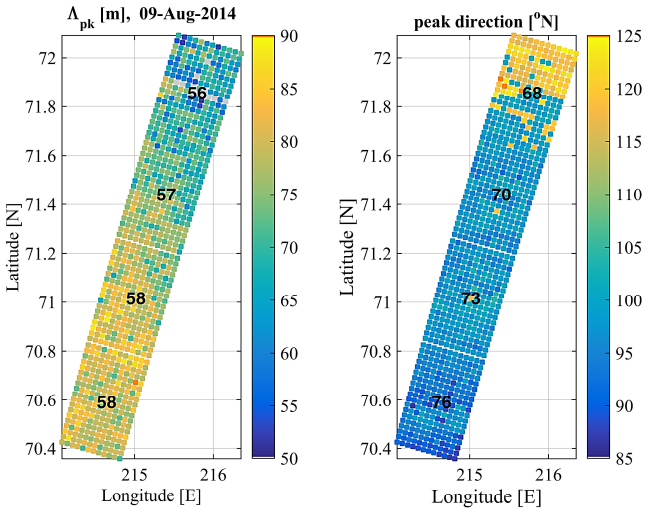

Fig. 2. Spatial heterogeneity of dominant wave length λ_{pk} (left) and dominant wave direction (right). Colour fields show results retrieved from TerraSAR-X Stripmap images, black numbers give Wavewatch III model results.

The retrieval of wind parameters from TerraSAR-X data takes the full nonlinear physical model function into account. At the same time the corresponding sea state can be estimated from the same image. The empirical model for obtaining integrated wave parameters is based on the analysis of image spectra, and uses parameters fitted with collocated buoy data and information on spectral peak direction and incidence angle. The algorithm derives significant wave height, wave direction and dominant wave length directly from SAR image spectra [4], [6]. Wave parameters are derived at approximately 2 km spatial resolution.

Wave parameters retrieved from the SAR images are compared to the output of the spectral wave model WAVEWATCH III [7]. The model is run with a polar stereographic grid, at $\approx 16km$ resolution, and uses the newest implementation of the ice source function S_{ice} implemented by NRL. Input fields of wind, and ice concentration and thickness are taken from the US Navy operational analyses.

3. RESULTS

Wind, wave and ice information has been retrieved from TS-X data in the marginal ice zones and open water conditions at diverse locations in the Arctic. Figures 1 - 2 shows an example from the Beaufort Sea, taken on August 9, 2014. At that time, an ice-free corridor had opened up along the entire width of the southern Beaufort Sea, allowing for long fetch conditions during easterly winds (Fig. 3). In-situ observations in the vicinity (not shown) indicate that the SAR images were taken during the decay phase of a substantial wave event with maximum significant wave heights of up to 3 m, which had decayed to about 2m during the time of our observation.

The satellite swath includes open water in its centre part, whereas the northern and southern ends are close to the retreating ice-edges. The significant wave height shows a wide range from about 1m closer to the northern ice edge to 2.3 m in the middle of the ice-free water section. Model results show a similar, but less pronounced trend. The vicinity of the ice can limit the fetch (the distance over which wave generation occurs), resulting in lower wave heights. This is likely the reason for the somewhat reduced wave heights in the southern region of the swath. The most pronounced drop in wave height is observed in the northern part of the satellite swath, most likely due to a combination of wave dampening in partial ice covered water, and short fetch conditions, and potentially somewhat weaker winds (Fig 1b). The dominant wave length is extracted from the peak of the 2-d wavenumber spectrum of the SAR image, and is therefore a direct observation (within the limits of the spectral resolution). Similar to the overall pattern of wave height, we see a slight gradient in wave length, from $> 80m$ in the south to $< 70m$ at the northern edge. The wave model gives shorter wave lengths, at approximately $60m$, and no variability. Dominant wave lengths from the model are calculated in the frequency space, and converted via the dispersion relation for short gravity waves to wave length: $\omega^2 = gk$, where ω, k are the wave frequency and wave number, respectively, and g is the acceleration due to gravity. This method has the inherent tendency of shorter dominant wave length obtained from the frequency space compared to values obtained from the wavenumber space, even for identical conditions [8]. How-

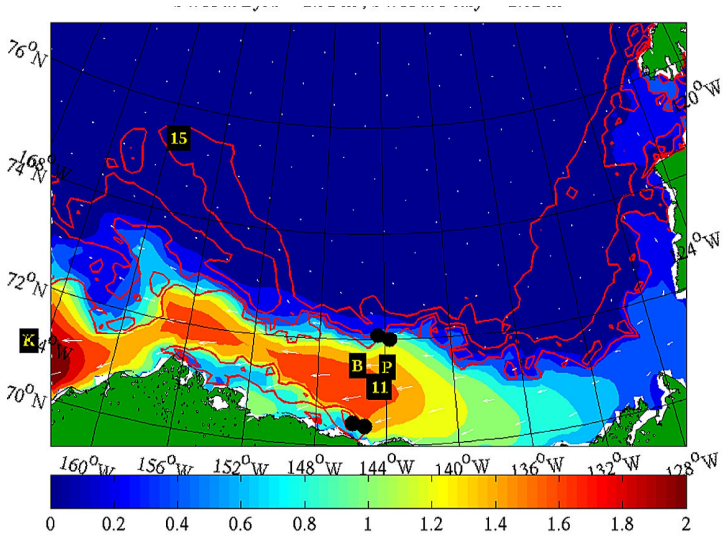

Fig. 3. Wavewatch III model results of significant wave height H_s, and input fields of wind speed (arrows) and ice concentration (25%, 50% and 75% contour lines).

ever, the expected difference is less than the differences observed here.

Dominant wave direction is from the East, with about 20^o discrepancy between the direction retrieved from the SAR image and the model output. The apparent jump of about 30^o within the northernmost 15 km of the satellite swath is not supported by the model result and might indicate contamination by remnant ice floes.

Further evaluation of the SAR wave and wind retrieval algorithms under different wind forcing and ice conditions, based on the entire data set, is ongoing. These results will also be included in testing and validation of new implementations of wind-wave-ice related processes in Wavewatch III.

The example discussed here highlights the strong spatial heterogeneity of the wave field in arctic regions, and the need for high resolution spatial wave observations.

Satellite-based wave field observations can bridge the gap between the single point buoy observation that provide high resolution time series of wave parameters, and the output of wave models which are of relatively coarse resolution and are inherently limited by the quality of the wind and ice input fields, but are unlimited in their spatial and temporal extent.

4. REFERENCES

[1] J. Thomson and W. Rogers, E., "Swell and sea in the emerging arctic ocean," *Geophys. Res. Let.*, vol. 10.1002/2014GL059983, pp. 3136–3140, 2014.

[2] J. Gemmrich, B R Thomas, and R. Bouchard, "Observational changes and trends in northeast pacific wave records," *Geophys. Res. Let.*, vol. 38, L22601, pp. doi:10.1029/2011GL049518, 2011.

[3] S. Lehner, A. Pleskachevsky, D. Velotto, and S Jacobsen, "Meteo-marine parameters and their variavbility observed by high-resolution satellite radar images," *Oceanography*, vol. 26, pp. 81–91, 2014.

[4] M. Bruck and S. Lehner, "Coastal wave field extraction using TerraSAR-X data," *Journal of Applied Remote Sensing*, vol. 7, pp. DOI: 10 .1117/1.JRS.7.073694], 2013.

[5] S. Lehner, A. L. Pleskachevsky, M. Bruck, X. Li, and S. Brusch, "Validation of coastal wind and wave fields by high resolution satellite data," in *12th International Workshop on Wave Hindcasting and Forecasting, Kohala Coast, Hawaii*, 2011.

[6] A. Pleskachevsky, C. Gebhardt, W. Rosenthal, S. Lehner, P. Hoffmann, J. Kieser, T. Bruns, A. Lindenthal, F. Jansen, and A. Behrens, "Satellite-based radar measurements for validation of highresolution sea state forecast models in the German Bight," in *ISRSE-36, 11-15 May 2015, Berlin, Germany. The International Archives of the Photogrammetry, Remote Sensing and Spatial Information Sciences, Volume XL-7/W3, 2015. doi:10.5194/isprsarchives-XL-7-W3-983-201.*, 2015.

[7] H. Tolman and the WAVEWATCH III Development Group, *User manual and system documentation of WAVEWATCH III, version 4.18*, National Oceanic and Atmospheric Administration National Weather Service National Centers for Environmental Prediction, 5830 University Research Court College Park, MD 20740, 2014.

[8] C. Gebhardt, A. Pleskachevsky, W. Rosenthal, S. Lehner, P. Hoffmann, J. Kieser, and T. Bruins, "Comparing wavelength simulated by coastal wave model CWAM and TerraSAR-X satellite data," *Ocean Modelling*, 2015.